Technical Note

Estimation of the Uncertainties Introduced in Thermal Map Mosaic: A Case of Study with PIX4D Mapper Software

Teresa Caputo *, Eliana Bellucci Sessa, Enrica Marotta, Antonio Caputo, Pasquale Belviso, Gala Avvisati, Rosario Peluso, Antonio Carandente

Posted Date: 14 July 2023

doi: 10.20944/preprints202307.0948.v1

Keywords: UAS; thermal images; surface temperature maps; thermal target

Technical Note

Estimation of the Uncertainties Introduced in Thermal Map Mosaic: A Case of Study with PIX4D Mapper Software

Teresa Caputo [1,*], Eliana Bellucci Sessa [1], Enrica Marotta [1], Antonio Caputo [1], Pasquale Belviso [1], Gala Avvisati [1], Rosario Peluso [1] and Antonio Carandente [1]

[1] Istituto Nazionale di Geofisica e Vulcanologia, Sezione di Napoli-Osservatorio Vesuviano, 80124 Naples, Italy; teresa.caputo@ingv.it (T.C.); eliana.bellucci@ingv.it (E.B.S.); enrica.marotta@ingv.it (E.M.); antonio.caputo@ingv.it (A.C. 1); pasquale.belviso@ingv.it (P.B.); gala.avvisati@ingv.it (G.A.); rosario.peluso@ingv.it (R.P.); antonio.carandente@ingv.it (A.C. 2);

* Correspondence: teresa.caputo@ingv.it; Tel.: +39-081-6108-216

Abstract: The aim of this study is to analyse problems related to thermal mapping obtained from thermal data acquired from Unmanned Aerial Systems (UAS) equipped with thermal cameras. We focused on an accurate analysis of uncertainties introduced by the PIX4D Mapper software used to obtain the surface temperature maps of thermal images acquired by the UAS. To achieve this aim, we used artificial thermal reference during the surveys, as well as natural hot targets, i.e. thermal anomalies in the Pisciarelli hydrothermal system in Campi Flegrei caldera (CFc). Artificial thermal targets, expressly created and designed for this goal, are a prototype here called "developed thermal target" (DTT) made by the drone Laboratory at Istituto Nazionale di Geofisica e Vulcanologia - Osservatorio Vesuviano (INGV-OV). We show the results obtained by three surveys during which thermal targets were positioned on land at different flight heights of the UAS. Different heights were also necessary to test spatial resolution of the DTT with the used thermal camera as well as possible temperature differences between the raw images acquired by UAS with the thermal mapping obtained from the PIX4D Mapper software. In this work we have estimated the uncertainty that may be introduced by the mosaic procedure and furthermore we find an attenuation of the measured temperatures introduced by the different distances between the thermal anomaly and sensor. These results appear to be of great importance for the subsequent calibration phase of the thermal maps especially in cases where these methodologies are applied for monitoring purposes of volcanic/geothermal areas.

Keywords: UAS; thermal images; surface temperature maps; thermal target

1. Introduction

In the last decades, thermal remote sensing techniques allowed the study, survey and analysis of the thermal behaviour of active volcanic areas [1–5]. The evolution of known thermal anomalies and the possible appearance of new areas with thermal anomalies are an indicator of changes in the volcanic systems, as it has been shown by recent studies [6–10].

In recent years the surface thermal behaviour of Campi Flegrei caldera (CFc; Southern Italy) has been monitored using different techniques in the field of thermal remote sensing. Different devices from portable/ground-based to UAS/satellite thermal infrared sensors [3–6,11–13] allowed the study and monitoring of the thermal anomalies linked to volcano activity at a local scale inside the CFc.

Since 2006, a permanent network for the monitoring of the ground thermal anomalies has been installed at CFc where diffuse degassing activity takes place [6,13–17]. Furthermore, ground temperature has been monitored and recorded since 2008 using handheld thermal cameras and since 2019 with the aid of UASs, with the main objective to identify any changes over time in the temperature values in discrete points and/or the identification of areas with a high temperature in order to highlight any change in the areal distribution of the fumarolic field and thermal anomalies [14,15,18–22].

For the type of fumarolic activity to be monitored, thermal imaging cameras acquire images both in RGB and in the infrared band (7.5-13.5 μm). Radiometric information is encoded as the fourth band in the images captured by the FLIR camera. Many available software, open source or commercial, have been developed to elaborate RGB images, while there are a lot less that are able to deal with radiometric images. PIX4D Mapper software [23] allows the use of radiometric images in the task of creating mosaics from data acquired by thermal cameras carried on UAS.

The present work aims to estimate the uncertainties introduced in thermal maps by the algorithms implemented in this photogrammetric software that are not known in literature at the present. For this purpose, the temperatures of the thermal targets, both artificial and natural, recorded on each single frame were compared with the corresponding temperatures on the resulting thermal map. Three different flights were performed in this study: the first in September 2020, when only natural thermal targets were used; the second and third in March 2021, when artificial thermal targets developed and implemented specifically to improve our analysis were also used. The testing area was Pisciarelli in the CFc near the Solfatara crater, which are the most active districts in CFc where the hydrothermal dynamics have been growing since 2012 [24].

The obtained results have great importance in the field of thermal sensing by UAS as they allow to use commercial mapping programs when creating thermal mosaic without introducing unknown or not estimated errors in the temperature of the obtained mapping.

2. Materials and Methods

The surveys were performed with UASs octocopters equipped with a FLIR Vue Pro R [25] with a resolution of 640x512 pixel and a focal length of 9mm (Table 1). The Vue Pro R camera gives its output in the FLIR proprietary Radiometric JPEGs format with radiometric data embedded for every pixel [25]. See Table 1 for technical details.

Table 1. Main characteristics of the UAS's Radiometric Thermal Camera Vue PRO R.

Model	Vue PRO R
Sensor Technology	Uncooled VOx Microbolometer
Weight	92 – 113.4g
Size	57.4 × 44.45 × 44.45mm (including lens)
Lens Options (FOV for Full-Sensor Digital Output)	9mm 69° × 56°
Resolution	640 × 512 pixel
Spectral band	7.5 - 13.5μm
Full Frame Rates	30 Hz (NTSC[1]); 25 Hz (PAL[2])
Measurement Accuracy	+/-5°C or 5% of reading
Accuracy	+/-5°C o 5% of reading in -25°C to +135°C range +/-20°C or 20% of reading in -40°C to +550°C range
Radiometric Data	Yes

[1] National Television Standard Committee; [2] Phase Alternating Line.

Three flights were analysed in the Pisciarelli area. All flights were performed in the evening/night when the sun's radiation is lower.

The first flight was carried out on September 14th, 2020 at a height of 70m, the other two carried out on March 8th, 2021 respectively at 55m and 70m above sea level.

Developed Thermal Targets (DTTs) were used for the two 2021 flights. The DTTs have been specially designed and built to have areas with a fixed and known temperature during the surveys. The DTTs are positioned on the ground and brought to the desired temperature before the flight, in order to be acquired and recorded by the camera during the flight. They are also useful to georeference thermal maps acquired with an UAS lacking an RTK (real-time kinematic) system [26].

 doi:10.20944/preprints202307.0948.v1

The acquired data were first analysed and then mosaicked using Pix4D Mapper (version 4.4.12, [23]), a photogrammetry software specific for thermal data. The natural thermal targets (NTTs) and DTTs were identified and subsequently an accurate check was carried out on the individual thermal frames containing the thermal targets. Finally the thermal maps obtained were imported into ArcGIS© [27] for statistical analysis on the same NTTs and DTTs.

2.1. Thermal target

Special DTTs have been conceived and developed by the staff of the Osservatorio Vesuviano, to support thermal surveys from UAS. Each target consists of a heated plate commonly used for 3D printers, linked to a digital thermostat with 12V 10A thermoregulator for temperature control across a temperature probe and management (sensor 8 in Figure 1) and a 12V 42AH battery (Figure 1). The dimensions of the targets has chosen according to:

- the resolution pixel on the ground of the thermal imaging camera during the flight;
- the set point temperature;
- the duration of the flight;
- the size of the battery that can be transported in the field during the investigations.

Figure 1. DTT target sketch.

To meet these requirements, 4 closely spaced thermal targets measuring 21x21 cm were positioned, so as to have a single target visible even at high flight altitudes. In this configuration, voids of about 4.5 cm are created on the short side and about 10cm on the long side of the rectangular grey box used for transport (see Figures 2 and 9, for example), giving the DTTs an overall final size of 46.5x52cm. This implies a reduction of the average temperature of the entire DTTs of approximately 27% due to unheated space between plates.

Preprints (www.preprints.org) | NOT PEER-REVIEWED | Posted: 14 July 2023 doi:10.20944/preprints202307.0948.v1

Figure 2. Positioning of DTTs during a survey. The grey box allows the transport of each single target assembled.

The thermal plates are able to reach a temperature of 90°C and are powered by a 12V battery drawing about 7A. These consumptions allow for an autonomy of about 5 hours with a 42Ah battery, taking into account the specific discharge curves of the connected battery [28]. The resistance of the board is approximately 1.6Ω. Each plate is connected to a thermostat (energy consumption < 3W) for temperature setting which has a temperature measurement range: -50°C ~ 99°C, an accuracy of ±0.1°C (-50°C ~ 70°C) and a resolution of 0.1°C (Figure 1). In Figure 2 is shown the positioning of the four plates while checking their temperature with the use of a handheld thermal FLIR SC640 (640x480 pixel, and accuracy of ±2°C) [29] during the survey.

In the case of volcanic and geothermal areas, in addition to DTTs natural thermal targets (NTTs) were also used, i.e. thermal anomalies naturally present in the area. In this last case, thermal anomalies of a quite regular geometric shape were chosen, such as those in correspondence of manholes (about diameter size of 1.30 m) as they are easily recognizable by shape and size of thermal anomalies.

2.2. Method of analysis

The present work wants to test the reliability of mosaic processing software and estimate the uncertainties that may occur in the thermal maps output. PIX4D Mapper photogrammetry software is used for thermal frame mosaics. The software processes the images following the principles of photogrammetry, i.e. it searches points clearly identify in two or more images (tie points) in adjacent images, and then uses them to link images and create a mosaic [23]. In particular, the choice of a software is constrained to the fact that it supports the radiometric images format acquired by the FLIR Vue Pro R and provides a mosaic thermal map (*Index Map)* using *Index Calculator*. The first step

Preprints (www.preprints.org) | NOT PEER-REVIEWED | Posted: 14 July 2023 doi:10.20944/preprints202307.0948.v1

consists of generating a 3D point cloud (Figure 3), then a 3D textured mesh (Figure 4) and finally the thermal *Index Map* selecting the band containing thermal data.

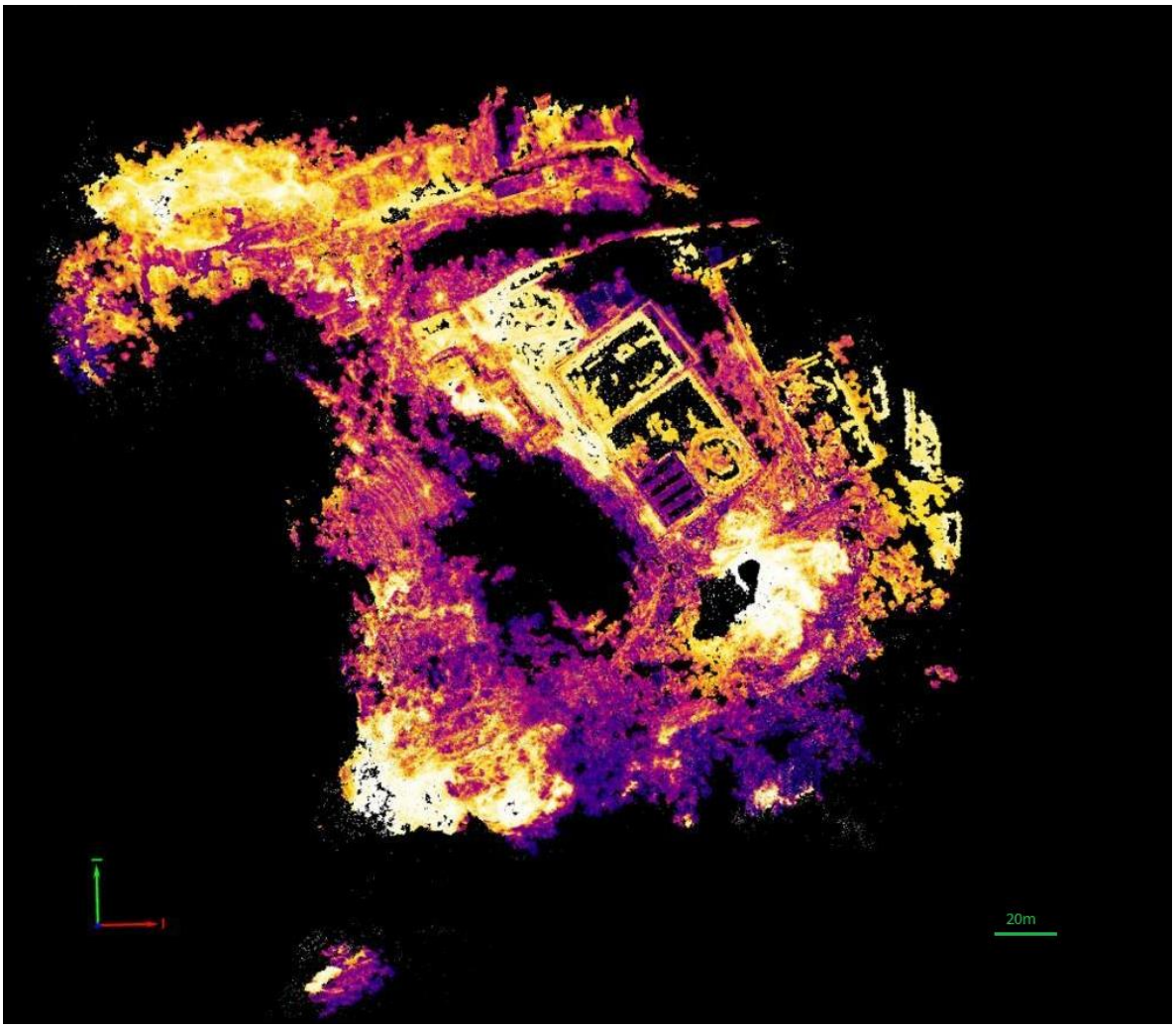

Figure 3. Thermal 3D points cloud of Pisciarelli area.

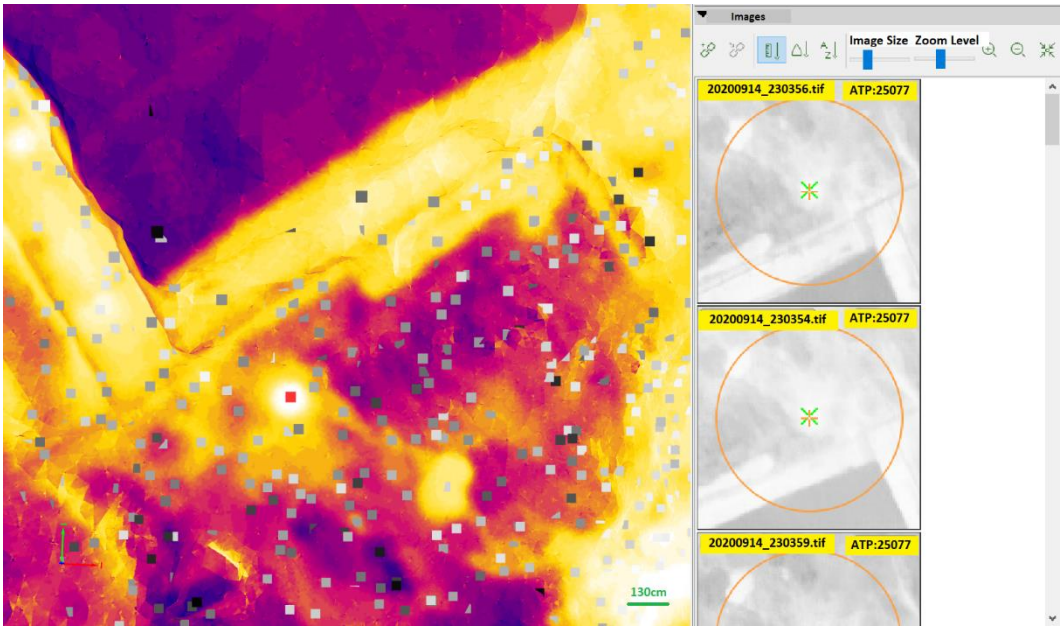

Preprints (www.preprints.org) | NOT PEER-REVIEWED | Posted: 14 July 2023 doi:10.20944/preprints202307.0948.v1

Figure 4. Detail of 3D thermal mesh on flying of September 14th, 2020. Red square identify the tie point related to manhole with its number of images marked on right.

To highlight natural thermal targets (NTTs) and/or artificial thermal targets (DTTs) graphical representations of the thermal *Index Map* were used at various temperature intervals (of 10°C) (Figure 5). In this way it was possible to recognize the targets, identify the relative tie points and go back to each single frame (Figure 4).

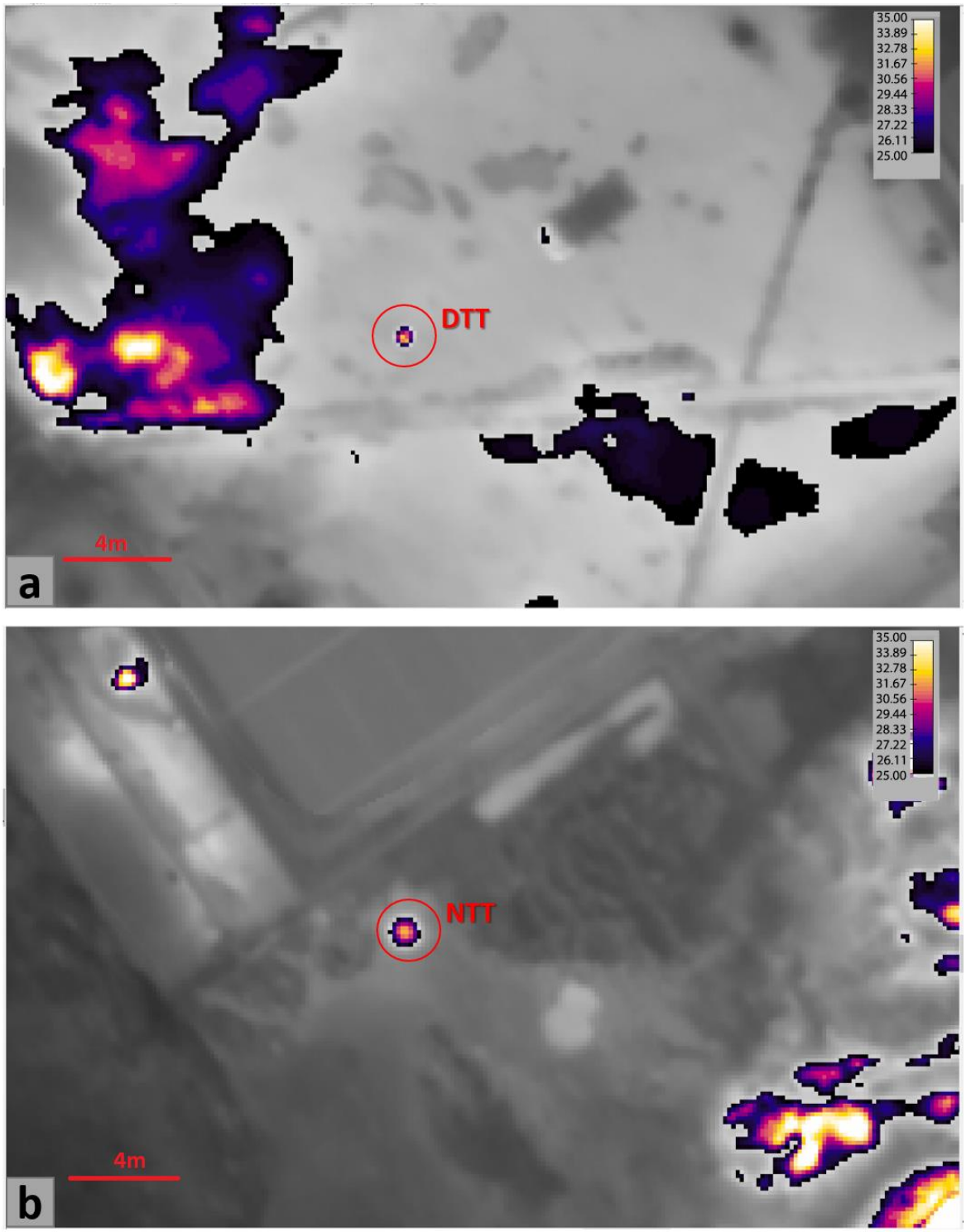

Figure 5. Detail of *Index Map*, fly of March 8th, 2021 at height of 70m, with temperature intervals between 25-35°C. In **a)** artificial thermal targets, DTT, are highlighted. In **b)** natural thermal anomalies, manhole NTT, are highlighted.

 doi:10.20944/preprints202307.0948.v1

Thus it was possible to compare the statistical analysis of the temperatures performed within the areas identifying the NTTs/DTTs on each original thermal frame with the statistical analysis of the temperatures obtained in the same areas on the thermal mosaic in the GIS environment (Figure 5).

FLIR's ThermaCAM Researcher software version 2.10 [30] was used for the statistical analysis of the DTTs/NTTs on the single frames, which allows to extract statistical information on the temperatures and to analyse in detail the minimum, maximum and average temperatures in the specific area on the thermal target (Figure 6). Statistical analysis is performed within an area; whereby geometric shapes have been generated around the NTTs/DTTs. The ability to generate simple geometric shape (such as squares and circles) allows for better accuracy when drawing the form of the recognized target. On every single frame that contains the thermal target, the same geometric shape has been recreated and within this form, statistical data have been calculated, such as the average temperature and its standard deviation σ. In the case of NTTs, the possibility of drawing simple geometric shapes (circle) repeatable in an identical way in the various frames is not always feasible. On the contrary, in the case of DTTs, their squared shape allows for a more easily reproducible geometry in the various frames.

Successively, the thermal *Index Map* has been imported in GIS Environment for detailed statistical analysis (Figures 7 and 8). Even in this case, the geometric shape containing the thermal target, both NTTs or DTTs, has been reproduced, within which the statistical information, such as minimum, maximum, range and mean on each area related to each thermal target.

Preprints (www.preprints.org) | NOT PEER-REVIEWED | Posted: 14 July 2023 doi:10.20944/preprints202307.0948.v1

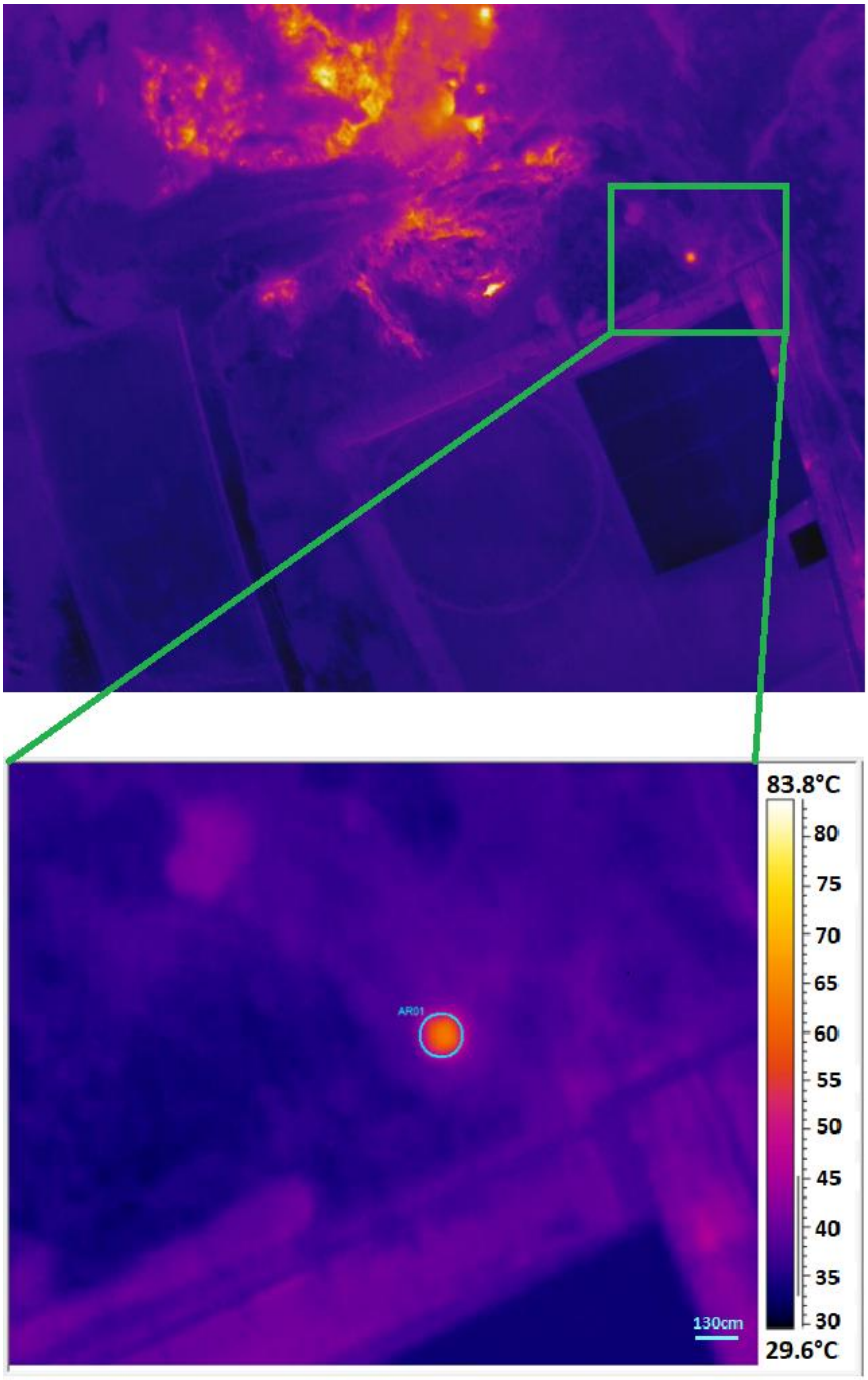

Figure 6. On top the original thermal frame acquired by UAS and on bottom recognition of the thermal target on individual frames. Case the manhole of the NTT reconstructed by circular geometric shape.

Preprints (www.preprints.org) | NOT PEER-REVIEWED | Posted: 14 July 2023 doi:10.20944/preprints202307.0948.v1

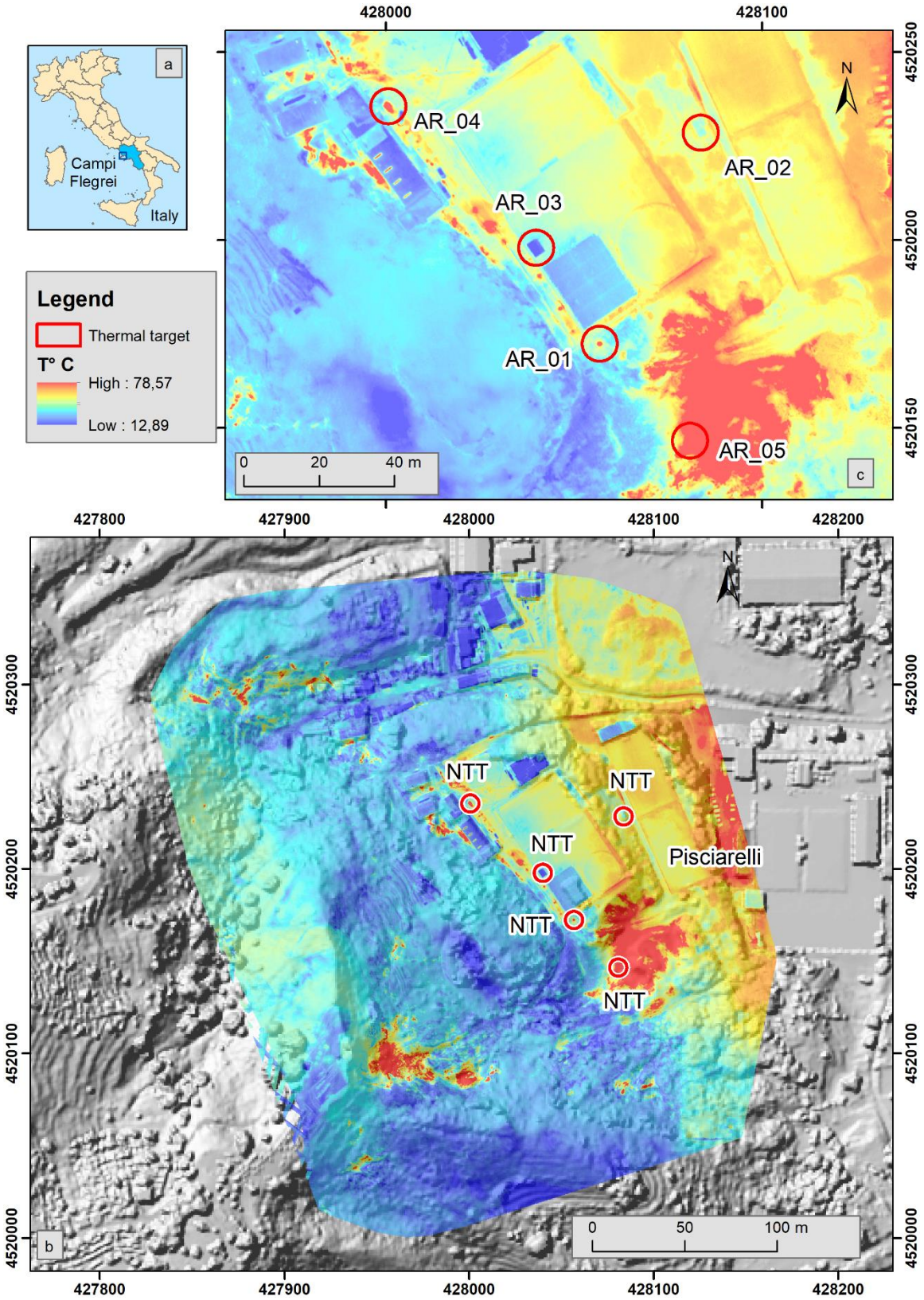

Figure 7. a) Location of study area; **b)** Digital Surface Model (DSM) of the geothermal Pisciarelli area with overlaid thermal map of fly of September 14th, 2020 at height of 70m; **c)** Detail of thermal map in GIS environment; the red circles highlight an example of the NTT identified on map. The colours on map represent the temperatures in °C as in the scale in the legend.

Preprints (www.preprints.org) | NOT PEER-REVIEWED | Posted: 14 July 2023 doi:10.20944/preprints202307.0948.v1

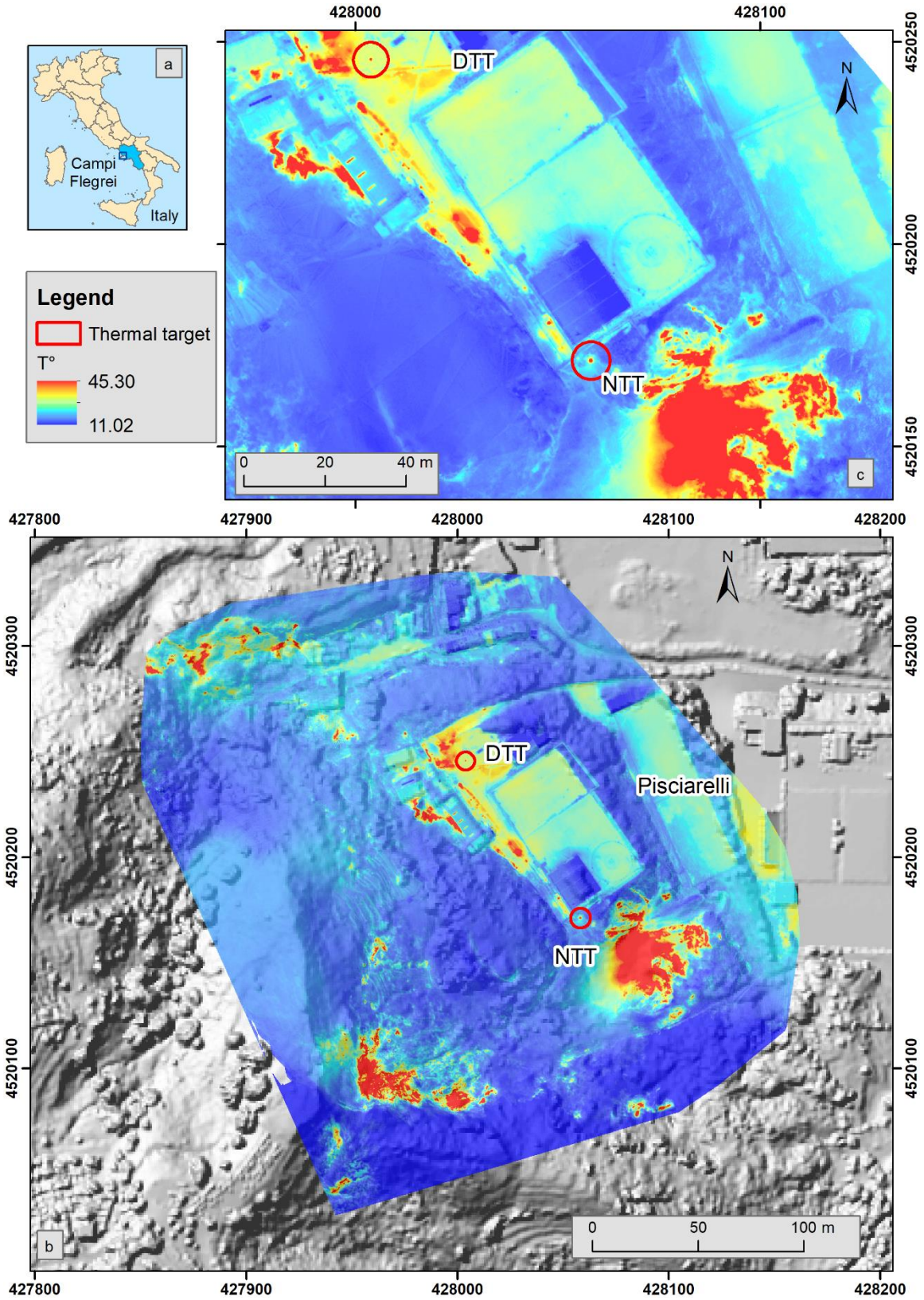

Figure 8. a) Location of study area; **b)** Digital Surface Model (DSM) of the geothermal Pisciarelli area with overlaid thermal map of fly of March 8th, 2021 at height of 55m; **c)** Detail of thermal map in GIS environment; red circles highlight an example of the DTT and NTT identified on map. The colours on map represent the temperatures in °C as in the scale in the legend.

Preprints (www.preprints.org) | NOT PEER-REVIEWED | Posted: 14 July 2023 doi:10.20944/preprints202307.0948.v1

3. Results

3.1. Survey of September 14th, 2020, 70m

Survey of September 14th, 2020 was performed at a height of 70m during the night, with an 80% (vertical) × 60% (horizontal) overlap; a total of 182 images were acquired with a pixel size at ground of 13.22cm. Only NTTs natural thermal targets were used during this test. To facilitate the recognition of NTTs on the thermal map, different intervals of representation of the temperature have been chosen on thermal *Index Map* and then five targets have been identified (AR0*) (Figure 7):

- AR01 highlighted on the thermal *Index Map* in the interval 40-50°C;
- AR02 highlighted on the thermal *Index Map* in the interval 30-40°C;
- AR03 highlighted on the thermal *Index Map* in the interval 20-30°C;
- AR04 highlighted on the thermal *Index Map* in the interval 50-60°C;
- AR05 highlighted on the thermal *Index Map* in the interval 60-70°C.

The tie points related to the five NTTs have a different associated thermal frame. The used geometrical shapes are different (circle or square) depending on the geometry of the selected NTT (Table 2). As previously mentioned, various representations of the thermal *Index Map* with only different temperature ranges have been made in order to highlight and isolate the clearly defined NTTs. Table 2 shows for each target the number of thermal frames identified by the software Pix4Dmapp for creating the mosaic, the average temperature weighted on all its frames (T_1) and calculated with ThermaCAM Researcher, the average temperature calculated on the output mapping (T_2) in GIS and their difference in absolute value.

Table 2. Weighted average and error on points NTTs of single thermal target, survey September 14th, 70m height. T_1 is the mean calculated with ThermaCAM Researcher over single NTTs, T_2 is the average temperature calculated on the thermal map in GIS.

Point	n° of frame	T_1 (°C) ± σ	T_2 (°C) ± σ	$\lvert T_1 - T_2 \rvert$(°C) ± σ
AR01	17	44.8 ± 0.2	46 ± 7	1 ± 7
AR02	10	33.36 ± 0.01	33.0 ± 0.6	0.3 ± 0.6
AR03	5	28.82 ± 0.02	27.2 ± 0.5	1.6 ± 0.4
AR04	20	53.98 ± 0.02	53 ± 5	1 ± 5
AR05	3	70.57 ± 0.04	64 ± 9	6 ± 9

3.2. Survey of March 8th, 2021, 70m

The survey of March 8th, 2021 was performed at a height of 70m during the evening, with an 80% (vertical) × 60% (horizontal) overlap; a total of 215 thermal images were acquired with a pixel size at ground of 13.22cm. During this test the 4 DTTs close together (DTTs joint) and one NTT (manhole) were used. The temperature of the manhole was measured with a handheld thermal camera (Figure 9) and resulted in about 40°C. The DTTs joint was placed on the ground by setting the maximum temperature of the probe point to 50°C (the probe is visible in Figure 9). A temperature dispersion due to the edge effect was measured on each plate, such as measured with a thermal handheld camera. In particular, the following average temperatures were recorded for each plate: 42.6°C, 43.5°C, 47°C, 43°C. Each plate has been mounted on a box, inside which the thermostat and the battery are stored during transport. This box, on the other hand generates a space and consequently an additional heat loss, due to the cold space between plates (see Figures 2 and 9). The average temperature of the DTT joint recorded by handheld thermal camera showed an average value of 41.2°C (± 8.9σ) (Figure 9). The dispersion due to the space between the 4 assembled plates determines a reduction of the average temperature of 6.4% (2.82°C) despite the cold area covering 27% of the total area.

Preprints (www.preprints.org) | NOT PEER-REVIEWED | Posted: 14 July 2023 doi:10.20944/preprints202307.0948.v1

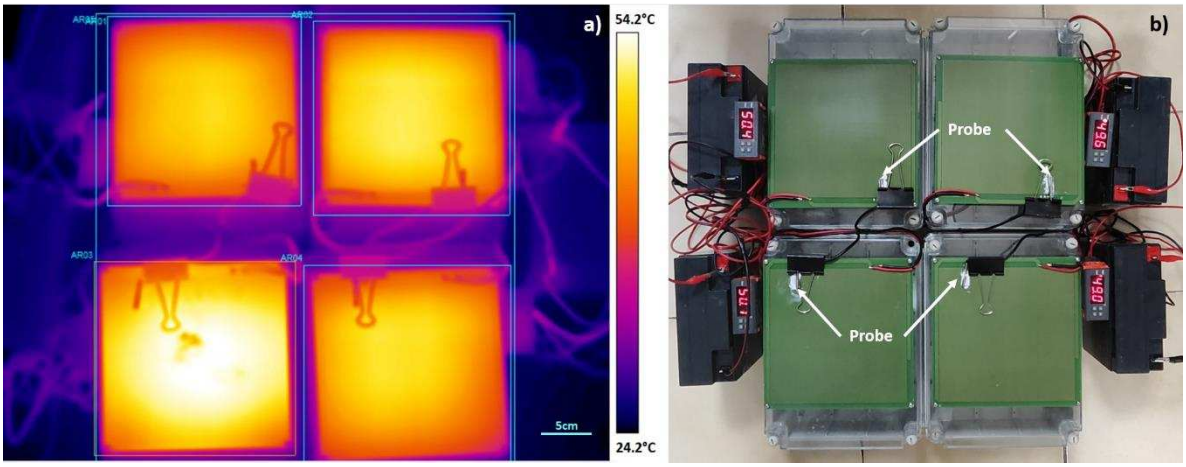

Figure 9. a) Thermal image of DTTs joint set all at 50°C. The box highlights the areas where temperatures have been calculated. b) Image of DTTs joint in RGB.

After various setting tests of temperature range to make it easier to recognize the DTTs on the thermal mapping, an interval of 10°C (25-35°C range) was chosen. For temperatures greater than 35°C the thermal targets are not visible.

The tie point related to the DTTs joint is associated with 26 thermal images. Then, with ThermaCAM Researcher software these images were analysed, searching in each of them the DTTs joint and reproducing its square shape. The tie point related to NTT (manhole) is associated to 8 thermal frames; in this case a circle was chosen to reproduce its geometric shape. For both targets, mean weighted and the relative error was calculated on all the recognized images, and then, in GIS environment, the average temperature was calculated on thermal map, T_2, as reported in Table 3.

Table 3. Weighted average and error on points DTT and NTT of single thermal frame, survey March 8th, 70m height, highlighted on thermal map 25-35°C.

Point	n° of frame	T_1 (°C) ± σ	T_2 (°C) ± σ	$\|T_1 - T_2\|$ (°C) ± σ
DTT	26	28.2 ± 0.3	30 ± 2	1 ± 2
NTT	8	27.6 ± 0.3	27 ± 3	1 ± 3

3.3. Survey of March 8th, 2021, 55m

On March 8th, 2021, a second fly was performed at a height of 55m, with an 80% (vertical) × 60% (horizontal) overlap; a total of 323 thermal images were acquired with a pixel size at ground of about 10.39cm. The DTTs joint and the NTT used are the same as the previous flight at 70m.

The tie points related to DTTs joint and NTT were associated with 28 and 8 thermal images, respectively. The weighted average and relative error are reported in Table 4. In this case the thermal targets were highlighted on the thermal map in the 20-40°C interval with GIS.

Table 4. Weighted average and error on points DTT and NTT of single thermal frame, survey March 8th, 55m height.

Point	n° of frame	T_1 (°C) ± σ	T_2 (°C) ± σ	$\|T_1 - T_2\|$(°C) ± σ
DTT	28	30.50 ± 0.02	32 ± 2	1 ± 2
NTT	8	27.4 ± 0.3	25 ± 3	2 ± 3

4. Discussion and conclusion

To evaluate the error that can be introduced on the temperature in a mosaic phase of the thermal frames, three flights were carried out and statistical analyses were performed both on the NTTs and on the DTTS. From the statistical analysis on the three flights carried out at different altitudes (two

flight at 70m and one at 55m) it emerges that the weighted average of the second and third flights (survey March 8th at 70m and 55m) have a maximum uncertainty of respectively ±3°C σ for the NTTs and of ±2°C σ for the DTTs (see Tables 3 and 4), while for the first flight (survey September 14th at 70m) the maximum uncertainty is ±9°C σ for NTTs (see Table 2). This great difference in the results could be attributed to the use of DTTs which allows a more accurate identification of the target itself and a better reconstruction of its geometry (having a well-known shape and size) allowing a more accurate and repeatable reconstruction on the various frames. Furthermore, the use of DTTs considerably reduces the error given by the difference between the averages of the single frames and the thermal mapping.

The error on the temperature difference (σ) is quite always greater than the difference itself (T_1 - T_2) meaning that it could be considered congruent with zero. Furthermore, giving a deeper look at the obtained data it is possible to identify as the main source of error the temperature distribution of the mapped thermal image. For these reasons we can infer that the algorithms that perform the mosaic process do not introduce in average temperatures an error bigger than the statistical one. Moreover, it is possible to see how this error results lower or equal to the measurement uncertainty of the Vue Pro (± 5°C or ± 55% in the used sensitivity interval, see technical data).

Furthermore, thanks to this experiment, it was noted that by comparing the temperature data acquired with the mobile thermal camera (manhole at 40°C and DTTs set at 50°C) with the images acquired during the flights and with the mobile thermal camera relative thermal mappings obtained, were observe an effect of attenuation on the temperatures of about 10°C. In particular, the DTTs that was set at 50°C (at the contact point of the sensor probe), shows an average temperature over the entire surface of about 41.2°C on the image acquired by the mobile camera (see Figure 9), while from the UAS thermal mapping the DTTs shows a mean temperature of about 30.50 (± 0.02 σ)for the 55m flight, with an uncertainty of ± 2°C σ and a mean temperature of 28.2°C (± 0.3 σ) for the 70m flight, with an uncertainty of ± 2°C σ. Similarly, the thermal images of the manhole acquired with the mobile thermal imager during the survey of March 8th give an average temperature of about 40°C for the 55m flight, while from the UAS thermal mapping it is of about 27.4 (± 0.3 σ) with an uncertainty of ± 3°C σ, while for the 70m flight it is of about 27.6 (± 0.3 σ) with an uncertainty of ± 3°C σ.

Finally, between flights at 55m and 70m there is an altitude difference of 15m (Δh= 15m) while the observed temperature variations between DTTs (30.50°C - 28.2°C) are 2.3°C. This implies a variation of 0.15°C for every meter of height. Similarly, the variation between the pixel size at ground at 55m and 70m is 2.83m, or 0.18m for each meter of height. The temperature differences between the DTTs target at ground level (1m), 41.2°C (± 8.9 σ) and at 55m, 30.5°C (± 0.02 σ), is 10.7°C, and that on 54m of elevation we find a decrease of 8.1°C (0.15°C x 54m), i.e. a difference between the calculated and measured values of (10.7-8.1°C) 2.6°C. Similarly, the temperature differences between the DTTs target ground level (1m), 41.2°C (± 8.9 σ) and at 70m, 28.2 (± 0.3 σ), is 13°C and that on elevation of 69m we find a decrease of 10.35°C, this implies that a difference between the calculated and the measured values of 2.5°C. The differences obtained (2.6°C for the flight at 55m and 2.5°C for the flight at 70m) are clearly lower than the error on the accuracy of the FLIR Vue Pro R (± 5°C) provided by the manufacturer.

4. This allows to calibrate the thermal mapping in the post-processing phase and to be able to evaluate more accurately the thermal anomalies especially in active geothermal/volcanic areas for the purposes of monitoring.

Author Contributions: Conceptualization, T.C., A.C.1 and R.P.; methodology, T.C.; software, T.C.; validation, T.C., E.B.S., and R.P.; formal analysis, T.C. and R.P.; investigation, P.B., G.A. and A.C.2; resources, E.M.; data curation, T.C.; writing—original draft preparation, T.C.; writing—review and editing, R.P., E.B.S. and E.M.; visualization, A.C.; supervision, E.M..; project administration, E.M.; funding acquisition, T.C. All authors have read and agreed to the published version of the manuscript.

Funding: This research received no external funding.

Conflicts of Interest: The authors declare no conflict of interest.

References

1. Harris, A. *Thermal Remote Sensing of Active Volcanoes: A User's Manual*; Cambridge University Press, 2013; ISBN 978-0-521-85945-5.
2. Calvari, S.; Lodato, L.; Spampinato, L. Monitoring Active Volcanoes Using a Handheld Thermal Camera. In Proceedings of the Thermosense XXVI; SPIE, April 12 2004; Vol. 5405, pp. 199–209.
3. Silvestri, M.; Marotta, E.; Buongiorno, M.F.; Avvisati, G.; Belviso, P.; Bellucci Sessa, E.; Caputo, T.; Longo, V.; De Leo, V.; Teggi, S. Monitoring of Surface Temperature on Parco Delle Biancane (Italian Geothermal Area) Using Optical Satellite Data, UAV and Field Campaigns. *Remote Sensing* **2020**, *12*, 2018, doi:10.3390/rs12122018.
4. Caputo, T.; Bellucci Sessa, E.; Silvestri, M.; Buongiorno, M.F.; Musacchio, M.; Sansivero, F.; Vilardo, G. Surface Temperature Multiscale Monitoring by Thermal Infrared Satellite and Ground Images at Campi Flegrei Volcanic Area (Italy). *Remote Sensing* **2019**, *11*, 1007, doi:10.3390/rs11091007.
5. Marotta, E.; Peluso, R.; Avino, R.; Belviso, P.; Caliro, S.; Carandente, A.; Chiodini, G.; Macedonio, G.; Avvisati, G.; Marfè, B. Remote Sensing Thermal Energy Release Measurement with Thermal Camera: The Case of La Solfatara Volcano (Italy). **2019**, doi:10.3390/rs11020167.
6. Vilardo, G.; Chiodini, G.; Augusti, V.; Granieri, D.; Caliro, S.; Minopoli, C.; Terranova, C. *The Permanent Thermal Infrared Network for the Monitoring of Hydrothermal Activity at the Solfatara and Vesuvius Volcanoes*; 2008;
7. Spampinato, L.; Oppenheimer, C.; Calvari, S.; Cannata, A.; Montalto, P. Lava Lake Surface Characterization by Thermal Imaging: Erta 'Ale Volcano (Ethiopia). *Geochemistry, Geophysics, Geosystems* **2008**, *9*, n/a-n/a, doi:10.1029/2008GC002164.
8. Spampinato, L.; Oppenheimer, C.; Cannata, A.; Montalto, P.; Salerno, G.G.; Calvari, S. On the Time-Scale of Thermal Cycles Associated with Open-Vent Degassing. *Bulletin of Volcanology* **2012**, *74*, 1281–1292, doi:10.1007/s00445-012-0592-2.
9. Marotta, E.; Calvari, S.; Cristaldi, A.; D'Auria, L.; Di Vito, M.A.; Moretti, R.; Peluso, R.; Spampinato, L.; Boschi, E. Reactivation of Stromboli's Summit Craters at the End of the 2007 Effusive Eruption Detected by Thermal Surveys and Seismicity. *Journal of Geophysical Research: Solid Earth* **2015**, *120*, 7376–7395, doi:10.1002/2015JB012288.
10. Vilardo, G.; Sansivero, F.; Chiodini, G. Long-Term TIR Imagery Processing for Spatiotemporal Monitoring of Surface Thermal Features in Volcanic Environment: A Case Study in the Campi Flegrei (Southern Italy). *Journal of Geophysical Research: Solid Earth* **2015**, *120*, 812–826, doi:10.1002/2014JB011497.
11. Cusano, P.; Caputo, T.; De Lauro, E.; Falanga, M.; Petrosino, S.; Sansivero, F.; Vilardo, G. Tracking the Endogenous Dynamics of the Solfatara Volcano (Campi Flegrei, Italy) through the Analysis of Ground Thermal Image Temperatures. *Atmosphere* **2021**, *12*, 940, doi:10.3390/atmos12080940.
12. Caputo, T.; Cusano, P.; Petrosino, S.; Sansivero, F.; Vilardo, G. Spectral Analysis of Ground Thermal Image Temperatures: What We Are Learning at Solfatara Volcano (Italy). In Proceedings of the Advances in Geosciences; Copernicus GmbH, September 11 2020; Vol. 52, pp. 55–65.
13. Sansivero, F.; Vilardo, G. Processing Thermal Infrared Imagery Time-Series from Volcano Permanent Ground-Based Monitoring Network. Latest Methodological Improvements to Characterize Surface Temperatures Behavior of Thermal Anomaly Areas. *Remote Sensing* **2019**, *11*, 553–553, doi:10.3390/rs11050553.
14. Aquino, I.; Augusti, V.; Avino, R.; Bagnato, E.; Bellomo, S.; Bellucci Sessa, E.; Belviso, P.; Benincasa, A.; Berrino, G.; Borgstrom, S.E.; et al. *Il Monitoraggio dei Vulcani Campani - Secondo semestre 2019*; 2021;
15. Aquino, I.; Augusti, V.; Avino, R.; Bagnato, E.; Bellomo, S.; Bellucci Sessa, E.; Belviso, P.; Benincasa, A.; Berrino, G.; Borgstrom, S.E.; et al. *Il Monitoraggio dei Vulcani Campani - Primo semestre 2019*; 2021;
16. Buongiorno, F.; Bellucci Sessa, E.; Caputo, T.; Silvestri, M. *CAMPI FLEGREI Monitoraggio Vulcanologico - Comparazione della temperatura superficiale da dati satellitari e Rete TIRNet*; Il Monitoraggio dei Vulcani Campani - Secondo semestre 2020; 2022; pp. 83–89;.
17. Buongiorno, F.; Bellucci Sessa, E.; Caputo, T.; Silvestri, M. *CAMPI FLEGREI Monitoraggio Vulcanologico - Comparazione della temperatura superficiale da dati satellitari e Rete TIRNet*; Il Monitoraggio dei Vulcani Campani - Primo semestre 2020; 2022; pp. 78–84;.
18. Della Seta, M.; Esposito, C.; Fiorucci, M.; Marmoni, G.M.; Martino, S.; Sottili, G.; Belviso, P.; Carandente, A.; de Vita, S.; Marotta, E.; et al. Thermal Monitoring to Infer Possible Interactions between Shallow

Hydrothermal System and Slope-Scale Gravitational Deformation of Mt Epomeo (Ischia Island, Italy). *Geological Society, London, Special Publications* **2022**, *519*, SP519-2020–2131, doi:10.1144/SP519-2020-131.

19. Cirillo, F.; Avvisati, G.; Belviso, P.; Marotta, E.; Peluso, R.; Pescione, R.A. Clustering of Handheld Thermal Camera Images in Volcanic Areas and Temperature Statistics. *Remote Sensing* **2022**, *14*, 3789, doi:10.3390/rs14153789.
20. Marotta, E.; Belviso, P.; Carandente, A.; Nave, R.; Peluso, R. *VESUVIO. Monitoraggio Termico con Termocamera Mobile e Termocoppia*; Il Monitoraggio dei Vulcani Campani - Primo semestre 2020; 2022; pp. 35–37;.
21. Marotta, E.; Belviso, P.; Carandente, A.; Nave, R.; Peluso, R. *CAMPI FLEGREI. Monitoraggio Termico con Termocamera Mobile e Termocoppia*; Il Monitoraggio dei Vulcani Campani - Secondo semestre 2020; 2022; pp. 78–82;.
22. Marotta, E.; Belviso, P.; Carandente, A.; Nave, R.; Peluso, R. *ISCHIA. Monitoraggio Termico con Termocamera Mobile e Termocoppia*; Il Monitoraggio dei Vulcani Campani - Secondo semestre 2020; 2022; pp. 117–122;.
23. PIX4Dmapper: Professional Photogrammetry Software for Drone Mapping Available online: https://www.pix4d.com/product/pix4dmapper-photogrammetry-software (accessed on 27 October 2022).
24. Caputo, T.; Mormone, A.; Marino, E.; Balassone, G.; Piochi, M. Remote Sensing and Mineralogical Analyses: A First Application to the Highly Active Hydrothermal Discharge Area of Pisciarelli in the Campi Flegrei Volcanic Field (Italy). *Remote Sensing* **2022**, *14*, 3526, doi:10.3390/rs14153526.
25. FLIR Vue Pro R | Teledyne FLIR Available online: https://www.flir.it/products/vue-pro-r?vertical=suas&segment=oem (accessed on 27 October 2022).
26. Langley, R.B. Rtk Gps. *Gps World* **1998**, *9*, 70–76.
27. ESRI ArcGIS, D. Release 10. *Redlands, CA: Environmental Systems Research Institute* **2011**, *437*, 438–438.
28. FGL_FOLDER_EMEA_ENG.Pdf Available online: https://www.fiamm.com/fileadmin//user_upload/FGL_FOLDER_EMEA_ENG.pdf (accessed on 7 December 2022).
29. User's Manual FLIR B6xx Series FLIR P6xx Series FLIR SC6xx Series Available online: https://support.flir.com/DocDownload/Assets/dl/1558550$a557.pdf (accessed on 7 December 2022).
30. ThermaCAM Researcher v2.10 | Imaging and Machine Vision Europe Available online: https://www.imveurope.com/press-releases/thermacam-researcher-v210 (accessed on 7 December 2022).